Available online at www.sciencedirect.com
SCIENCE DIRECT®
Journal of Sound and Vibration 270 (2004) 149–169
JOURNAL OF SOUND AND VIBRATION
www.elsevier.com/locate/jsvi

# A spectral element for laminated composite beams: theory and application to pyroshock analysis

R. Ruotolo*

*Department of Aerospace Engineering, Politecnico di Torino, corso Duca degli Abruzzi 24, Torino, Italy*

Received 2 August 2002; accepted 7 January 2003

**Abstract**

In this article a spectral element for anisotropic, laminated composite beams is developed. Firstly, the axial-bending coupled equations of motion are derived under the assumptions of the First order Shear Deformation Theory, then the spectral element matrix is formulated. The proposed spectral element is validated by comparing, with corresponding results from the scientific literature, natural frequencies of a number of both orthotropic and anisotropic laminated composite beams and the dynamic response of an anisotropic cantilever beam to high frequency transients. Finally, the application of the proposed element to the evaluation of the dynamic response to a simulated pyroshock of an idealized satellite structure made of sandwich beams is shown.


## 1. Introduction

Composite materials offer a number of advantages with respect to isotropic ones thanks to their low density and to the possibility of optimizing their strength and stiffness by properly determining the fibre orientation of every layer into the laminate. As a result, the analysis of their static and dynamic behaviour is a very active research area in particular in the aerospace engineering field, where the minimization of the structural mass is one of the first objectives of the design.

The necessity to predict high frequency structural vibrations is typical of structure-borne sound and noise transmission, as well as of problems characterized by exciting forces with very large bandwidth, such as impacts and pyroshocks. As underlined in Ref. [1], impacts are a very crucial topic for laminated composite structures, because discontinuous bending stress gradients at the ply interfaces may cause delamination or debonding of the layers.

*Currently employed at Fiat GM Powertrain Italia.
*E-mail address:* romualdo.ruotolo@it.fiat-gm-pwt.com (R. Ruotolo).

0022-460X/03/$ - see front matter 
doi:10.1016/S0022-460X(03)00488-7

On the other side, due to the highly probable more extensive use of composite materials in future primary and secondary space structures, pyroshock prediction in composites is a topic that may become of great importance during the next years. As described in Ref. [2] launch vehicles and spacecraft make large use of pyrotechnic charges to deploy appendices (e.g., antennas) or separate subsystems (e.g., disconnect valves). Nevertheless, these charges have the drawback of giving rise to transients, called pyroshocks, that propagate through primary and secondary structures and are characterized by very short duration (less than 20 ms), extremely high accelerations (up to 300 000 $g$ [3]) and very large bandwidth. Usually small components, such as electronic boards, are very sensitive to these transients, so that their accurate prediction is of great importance for the success of the mission.

All these problems can be investigated by taking advantage of the concept of wave propagation in structural media, as demonstrated by Cremer et al. [4] about structure-borne sound transmission and by Doyle [5] about transient prediction. Nevertheless, it must be stressed that it is necessary to base the techniques presented in these books on valid mathematical models of laminated composite structures in the frequency range under analysis to obtain accurate results.

Static and dynamic behaviour of laminated composite beams has been investigated by a number of researchers who have developed several theories: from simple ones, e.g., those based on Euler–Bernoulli assumptions, to those considering transverse normal stress components. A review of them, strictly related to beams only, is given by Marur and Kant in Refs. [6,7].

Moreover, it can be recalled that equations of motion for beams can be derived from those of elastic shells under some simplifying assumptions (e.g., in both Refs. [8,9] it is shown that equations of motion for laminated beams can be derived from those of laminated plates). As a result, it is possible to refer to developments in the theory of elastic shells to briefly review corresponding beam theories.

Laminate thin elastic shells have been examined by several investigators. Usually, the problem of determining the static and dynamic response, as well as the dynamic behaviour, of laminate and/or homogeneous isotropic shells is addressed by using some simplifying assumptions proposed initially by Love that led to the development of a sub-class of the theory of elasticity known as the theory of thin elastic shells. Love's First Approximation Theory (LFAT) for thin elastic shells is based upon the following postulates [10]: (1) the shell is thin, (2) the deflections of the shell are small, (3) the transverse normal stress is negligible, (4) normals to the middle surface of the shell remain normal to it and undergo no change in length during deformation. The well-known Classical Lamination Theory (CLT) [11] is based on the previous four postulates.

As described by Reddy [8,12] several other theories have been developed by delaying the fourth Love's postulate. For thick laminates and laminates with high degree of anisotropy, transverse deformation effects can be significant and theories which hold the fourth postulate are not able to determine accurately the response to static and dynamic loads. As a consequence, First order Shear Deformation Theories (FSDT) have been developed, which consider a constant transverse shear strain over the thickness of the laminate [12]; this is the equivalent of the Timoshenko theory for isotropic beams. In contrast, Second and Higher order SDT use higher order polynomials to describe displacement components through the thickness of the laminate. Finally, some refined theories have been introduced to fulfill shear stress continuity

and consider the distortion of the deformed normal, e.g., that proposed by Di Sciuva in Ref. [13].

A number of researchers compared these theories from both the static and the dynamic point of view; prevailing results are summarized in Refs. [8,9]. Moreover, Marur and Kant [6] compared higher order refined theories on the transient response of laminated composite beams, showing the effects of shear deformation and rotatory inertia. In general, all these studies put in evidence the central role of the thickness to length ratio ($h/L$) as the criterion to be used for selecting the most appropriate theory.

Furthermore, it must be stressed that also the frequency range of the excitation influences the theory to be used. This has been shown by Cremer et al. [4], where they compared Euler–Bernoulli and Timoshenko theories for isotropic beams. Under the assumption that the former can be used when it predicts the propagation velocity of a sinusoidal wave with an error lower than 10%, they demonstrated that the Euler–Bernoulli theory provides accurate results when the wavelength, $\lambda$, is greater than six times the thickness, $h$, of the beam under analysis. As a result, shear deformation and rotatory inertia effects must be taken into account in a proper way at high frequencies, where the $\lambda/h > 6$ condition is not respected.

Spectral elements have been proposed by Doyle [5] to study the wave propagation in structures. Their main feature is the use of exact shape functions, permitting one to describe exactly the mass distribution within a structural element; as a result, the spectral element matrix is equal to the so-called dynamic stiffness matrix [14] relating generalized forces to displacements at the nodes of the element under consideration. Nevertheless, it must be stressed that the spectral element matrix and the dynamic stiffness are derived by using different approaches. Indeed the former is derived by assuming wave motion into the structural element, requiring the solution of the corresponding dispersion relation. In contrast, the dynamic stiffness matrix is based on the assumption of harmonic motion so that the resulting differential problem depends on space variables only (see e.g., Eisenberger et al. [15] and Abramovich et al. [16] where the displacements field is defined as an infinite and convergent recurring series, and Ref. [17] where Leung and Zhou used the Kantorovich method).

The direct consequence of the use of exact shape functions is the ability of the Spectral Element Method (SEM) to deal with high frequency problems, where associated wavelengths become very small. This property makes SEM very attractive from the computational point of view, in particular for those problems in which the exciting force has a very large bandwidth. In contrast, the Finite Element Method (FEM) requires a huge number of elements to match the smallest characteristic wavelength of the problem.

At the moment, spectral element formulations are available only for few structural elements. By focusing the attention on beam structures, in Ref. [5] a Timoshenko beam for isotropic material is presented, in Ref. [18] dynamic properties of piezoelectric actuated beams are analyzed, while Mahapatra et al. proposed in Ref. [1] a spectral element for Euler–Bernoulli (i.e., based on CLT assumptions) composite beams.

As a result, the aim of this article is to extend the library of spectral elements currently available by determining the spectral element matrix for an anisotropic, composite laminated beam based on the First Shear Deformation Theory (i.e., the equivalent of the Timoshenko theory for composite laminates), making SEM applicable to deal with relatively thick composite and sandwich structures.

## 2. Formulation of the spectral element

### 2.1. Equations of motion and boundary conditions

An anisotropic, laminated composite beam with width $b$, thickness $h$ and length $L$ is considered. It is assumed that each layer of the laminated beam behaves macroscopically as a homogeneous, orthotropic, linearly elastic material and all layers are assumed to be perfectly bonded together. Moreover, the co-ordinates are oriented so that $x$ is directed along the beam axis and $z$ along its thickness. Under the assumptions of the FSDT [12] in-plane, $u(x,z)$, and out-of-plane, $w(x,z)$, displacements of the beam are given by

$$\begin{aligned} u(x,z) &= u_0(x) + z\phi(x), \\ w(x,z) &= w(x), \end{aligned} \tag{1}$$

where $u_0(x)$ is the mid-plane axial displacement, $\phi(x)$ is the rotation of the cross-section and the second equation states that there is no contraction along the out-of-plane direction.

By applying the well-known rules leading to deformations, it follows:

$$\begin{aligned} \varepsilon_x &= \varepsilon_0 + zk_x = u_{0,x} + z\phi_{,x}, \\ \gamma_{xz} &= w_{,x} + \phi, \end{aligned} \tag{2}$$

where $(\cdot)_{,x} = \partial(\cdot)/\partial x$.

Deformations are related to traction, $N$, bending moment, $M$, and shear, $Q$, according to

$$\begin{aligned} \begin{Bmatrix} N \\ M \end{Bmatrix} &= \begin{bmatrix} A_{11} & B_{11} \\ B_{11} & D_{11} \end{bmatrix} \begin{Bmatrix} \varepsilon_0 \\ k_x \end{Bmatrix}, \\ Q &= KA_{55}\gamma_{xz}\,, \end{aligned} \tag{3}$$

where $K$ is the shear correction factor and rigidities $A_{11}$, $B_{11}$ and $D_{11}$ are derived according to Reddy [8], i.e., considering the Poisson effect by starting from corresponding quantities determined for plates and recalling that $N_{yy} = N_{xy} = M_{yy} = M_{xy} = 0$.

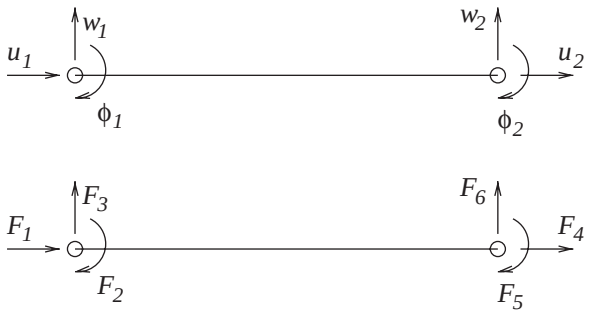


Fig. 1. The spectral element under consideration: generalized displacements (upper) and forces (lower).

By considering both effects of inertia load and of generalized forces $F_1, \ldots, F_6$ shown in Fig. 1, the virtual work principle gives

$$\int_0^L (N\delta\varepsilon_0 + M\delta k_x + Q\delta\gamma_{xz})\,\mathrm{d}x + b\int_0^L \int_{-h/2}^{h/2} \rho(z)(\ddot{u}(x,z)\delta u(x,z) + \ddot{w}(x,z)\delta w(x,z))\,\mathrm{d}x\,\mathrm{d}z + \\ - F_1\delta u_0(0) - F_4\delta u_0(L) - F_2\delta\phi(0) - F_5\delta\phi(L) - F_3\delta w(0) - F_6\delta w(L) = 0. \tag{4}$$

By introducing

$$I_n = b\int_{-h/2}^{h/2} \rho(z) z^n\,\mathrm{d}z \tag{5}$$

recalling Eq. (1), integrating Eq. (4) by parts, the equations of motion are derived:

$$\begin{aligned} &- N_{,x} + I_0\ddot{u}_0 + I_1\ddot{\phi} - I_1\ddot{w}_{,x} = 0,\\ &- M_{,x} + Q + I_1\ddot{u}_0 + I_2\ddot{\phi} - I_2\ddot{w}_{,x} = 0,\\ &- Q_{,x} + I_0\ddot{w} = 0 \end{aligned} \tag{6}$$

associated with the following natural boundary conditions:

$$\begin{Bmatrix} F_1\\ F_2\\ F_3 \end{Bmatrix} = -\begin{Bmatrix} N(0)\\ M(0)\\ Q(0) \end{Bmatrix}, \qquad \begin{Bmatrix} F_4\\ F_5\\ F_6 \end{Bmatrix} = \begin{Bmatrix} N(L)\\ M(L)\\ Q(L) \end{Bmatrix}. \tag{7}$$

### 2.2. Governing wave equations

Under the assumption of wave propagation into laminated beams, generalized co-ordinates can be written as

$$\begin{Bmatrix} u_0(x,t)\\ \phi(x,t)\\ w(x,t) \end{Bmatrix} = \begin{Bmatrix} U\\ P\\ W \end{Bmatrix} \mathrm{e}^{\mathrm{i}kx}\mathrm{e}^{\mathrm{i}\omega t}, \tag{8}$$

where $k$ is the wavenumber and $\omega$ is the circular frequency. By introducing the previous relation into the equations of motion (6), and taking advantage of relation (3), it is possible to determine for each circular frequency $\omega$ the wavenumber, $k_n$, and the corresponding shape (in terms of coefficients $U_n$, $P_n$ and $W_n$) of waves propagating into the beam at that frequency. The consequent system of equations is the following:

$$\begin{bmatrix} (A_{11}k^2 - I_0\omega^2) & (B_{11}k^2 - I_1\omega^2) & 0\\ (B_{11}k^2 - I_1\omega^2) & (D_{11}k^2 + KA_{55} - I_2\omega^2) & \mathrm{i}KA_{55}k\\ 0 & -\mathrm{i}KA_{55}k & (KA_{55}k^2 - I_0\omega^2) \end{bmatrix} \begin{Bmatrix} U\\ P\\ W \end{Bmatrix} = \begin{Bmatrix} 0\\ 0\\ 0 \end{Bmatrix}. \tag{9}$$

By setting a circular frequency $\omega$, the previous system of equations is satisfied by values of $k$ that are eigenvalues of the coefficient matrix. Since powers up to 2 of $k$ are present in the coefficient matrix, to simplify the evaluation of eigenvalues, the previous equation is

rewritten as

$$\left(\sum_{m=0}^{2}[\mathbf{M}_m]k^m\right)\left\{\begin{array}{c}U\\P\\W\end{array}\right\}=\left\{\begin{array}{c}0\\0\\0\end{array}\right\} \tag{10}$$

with

$$[\mathbf{M}_0]=\begin{bmatrix}-I_0\omega^2 & -I_1\omega^2 & 0\\ -I_1\omega^2 & KA_{55}-I_2\omega^2 & 0\\ 0 & 0 & -I_0\omega^2\end{bmatrix},$$

$$[\mathbf{M}_1]=\begin{bmatrix}0 & 0 & 0\\ 0 & 0 & \mathrm{i}KA_{55}\\ 0 & -\mathrm{i}KA_{55} & 0\end{bmatrix},$$

$$[\mathbf{M}_2]=\begin{bmatrix}A_{11} & B_{11} & 0\\ B_{11} & D_{11} & 0\\ 0 & 0 & KA_{55}\end{bmatrix}.$$

Eq. (10) can be solved by taking advantage of the companion matrix concept, i.e., rewriting Eq. (10) as

$$[\boldsymbol{\alpha}]\{\hat{\mathbf{G}}_n\}-k_n[\boldsymbol{\beta}]\{\hat{\mathbf{G}}_n\}=\{\mathbf{0}\} \tag{11}$$

with

$$[\boldsymbol{\alpha}]=\begin{bmatrix}[\mathbf{0}] & [\mathbf{I}]\\ [\mathbf{M}_0] & [\mathbf{M}_1]\end{bmatrix},$$

$$[\boldsymbol{\beta}]=\begin{bmatrix}[\mathbf{I}] & [\mathbf{0}]\\ [\mathbf{0}] & -[\mathbf{M}_2]\end{bmatrix},$$

$$\{\hat{\mathbf{G}}_n\}^{\mathrm{T}}=\lfloor\, k_n^0\{\mathbf{G}_n\}^{\mathrm{T}} \quad k_n^1\{\mathbf{G}_n\}^{\mathrm{T}}\,\rfloor^{\mathrm{T}} \qquad \{\mathbf{G}_n\}^{\mathrm{T}}=\lfloor\, U_n\ P_n\ W_n\,\rfloor^{\mathrm{T}}$$

in which [0] is the $(3\times 3)$ null matrix and $[\mathbf{I}]$ is the $(3\times 3)$ identity matrix.

As a result, six wavenumbers $k_n$, for a given circular frequency, are evaluated as eigenvalues of the matrix $[\boldsymbol{\beta}]^{-1}[\boldsymbol{\alpha}]$, that is non-singular because matrix $[\mathbf{M}_2]$ cannot be singular. Corresponding eigenvectors, i.e., shapes of propagating waves $\{\mathbf{G}_n\}^{\mathrm{T}}=\lfloor\, U_n\ P_n\ W_n\,\rfloor^{\mathrm{T}}$, are given by the first three elements of $\{\hat{\mathbf{G}}_n\}$.

It follows that at the selected circular frequency, $\omega$, displacements can be written as a superposition of six waves:

$$\left\{\begin{array}{c}u_0(x,t)\\ \phi(x,t)\\ w(x,t)\end{array}\right\}=\sum_{n=1}^{6}a_n\left\{\begin{array}{c}U_n\\ P_n\\ W_n\end{array}\right\}\mathrm{e}^{\mathrm{i}k_nx}\mathrm{e}^{\mathrm{i}\omega t} \tag{12}$$

that can be reorganized as

$$\begin{Bmatrix} u_0(x,t) \\ \phi(x,t) \\ w(x,t) \end{Bmatrix} = [\mathbf{\Phi}][\boldsymbol{\lambda}(x)]\{\mathbf{a}\}e^{i\omega t}, \tag{13}$$

where $\{\mathbf{a}\}^T = \lfloor a_1 \ldots a_6 \rfloor^T$ and

$$[\mathbf{\Phi}] = [\{\mathbf{G}_1\} \ \ldots \ \{\mathbf{G}_6\}],$$

$$[\boldsymbol{\lambda}(x)] = \begin{bmatrix} e^{ik_1 x} & & \\ & \ddots & \\ & & e^{ik_6 x} \end{bmatrix}.$$

### 2.3. Spectral element shape functions

The spectral element of the anisotropic laminated composite beam under consideration is characterized by the generalized degrees of freedom (d.o.f.s) represented in Fig. 1, i.e., axial displacement, cross-section rotation and vertical displacement at both ends.

In order to derive the shape functions of this element, the approach described by Doyle [5] is used. Accordingly, by evaluating the displacements given by Eq. (13) at $x = 0$ and $L$ it is possible to determine the relation between constants $\{\mathbf{a}\}$ and the generalized d.o.f.s at the left and right end of the beam respectively:

$$\begin{Bmatrix} u_1 \\ \phi_1 \\ w_1 \end{Bmatrix} = [\mathbf{\Phi}]\{\mathbf{a}\} \tag{14}$$

and

$$\begin{Bmatrix} u_2 \\ \phi_2 \\ w_2 \end{Bmatrix} = [\{\mathbf{G}_1\}e^{ik_1 L} \ \ldots \ \{\mathbf{G}_6\}e^{ik_6 L}]\{\mathbf{a}\} = [\hat{\mathbf{\Phi}}]\{\mathbf{a}\}. \tag{15}$$

These last two equations can be rewritten as

$$\{\mathbf{V}\} = \begin{bmatrix} [\mathbf{\Phi}] \\ [\hat{\mathbf{\Phi}}] \end{bmatrix}\{\mathbf{a}\} = [\mathbf{F}]^{-1}\{\mathbf{a}\},$$

where vector $\{\mathbf{V}\}$ collects the six generalized d.o.f.s. As a result, the displacements can be written as

$$\begin{Bmatrix} u_0(x,t) \\ \phi(x,t) \\ w(x,t) \end{Bmatrix} = [\mathbf{\Phi}][\boldsymbol{\lambda}(x)][\mathbf{F}]\{\mathbf{V}\}e^{i\omega t}, \tag{16}$$

where $[\mathbf{\Phi}][\boldsymbol{\lambda}(x)][\mathbf{F}]$ gives the shape functions of the spectral element.

### 2.4. Spectral element matrix

As shown by Doyle [5], the spectral element matrix can be derived by firstly evaluating generalized displacement derivatives, then the stress resultants $N$, $M$ and $Q$ according to Eq. (3) and finally external forces by using relation (7).

In order to determine generalized displacements derivative, the following matrix must be introduced:

$$[\boldsymbol{\lambda}'(x)] = \begin{bmatrix} \mathrm{i}k_1 \mathrm{e}^{\mathrm{i}k_1 x} & & \\ & \ddots & \\ & & \mathrm{i}k_6 \mathrm{e}^{\mathrm{i}k_6 x} \end{bmatrix}$$

so that

$$\begin{Bmatrix} u_{0,x}(x) \\ \phi_{,x}(x) \\ w_{,x}(x) \end{Bmatrix} = [\boldsymbol{\Phi}][\boldsymbol{\lambda}'(x)][\mathbf{F}]\{\mathbf{V}\}. \tag{17}$$

As a result, the stress resultants are given by

$$\begin{aligned} \begin{Bmatrix} N(x) \\ M(x) \\ Q(x) \end{Bmatrix} &= \begin{bmatrix} A_{11} & B_{11} & 0 \\ B_{11} & D_{11} & 0 \\ 0 & 0 & KA_{55} \end{bmatrix} \begin{Bmatrix} u_{0,x} \\ \phi_{,x} \\ w_{,x} + \phi \end{Bmatrix} \\ &= \begin{bmatrix} A_{11} & B_{11} & 0 \\ B_{11} & D_{11} & 0 \\ 0 & 0 & KA_{55} \end{bmatrix} ([\mathbf{I}][\boldsymbol{\Phi}][\boldsymbol{\lambda}'(x)] + [\mathbf{I}_\phi][\boldsymbol{\Phi}][\boldsymbol{\lambda}(x)])[\mathbf{F}]\{\mathbf{V}\} \\ &= [\mathbf{R}][\mathbf{S}(x)][\mathbf{F}]\{\mathbf{V}\}, \end{aligned} \tag{18}$$

where

$$[\mathbf{I}_\phi] = \begin{bmatrix} 0 & 0 & 0 \\ 0 & 0 & 0 \\ 0 & 1 & 0 \end{bmatrix}.$$

By recalling Eq. (7) and using Eq. (18), external forces and d.o.f.s are related by

$$\begin{Bmatrix} F_1 \\ F_2 \\ F_3 \end{Bmatrix} = -[\mathbf{R}][\mathbf{S}(0)][\mathbf{F}]\{\mathbf{V}\} \tag{19}$$

and

$$\begin{Bmatrix} F_4 \\ F_5 \\ F_6 \end{Bmatrix} = [\mathbf{R}][\mathbf{S}(L)][\mathbf{F}]\{\mathbf{V}\} \tag{20}$$

so that the dynamic stiffness matrix of the spectral element is given by

$$[\mathbf{K}_d] = [\mathbf{R}] \begin{bmatrix} -[\mathbf{S}(0)] \\ [\mathbf{S}(L)] \end{bmatrix} [\mathbf{F}]. \tag{21}$$

## 3. Numerical results

### 3.1. Numerical validation: natural frequencies

In order to validate the spectral element proposed in the previous section, a number of comparisons with published corresponding results are shown. All layers of each of the following beams have the same thickness, moreover it is assumed that every orthotropic lamina has the following material properties: $E_1 = 144.8$ GPa, $E_2 = 9.65$ GPa, $G_{12} = G_{13} = 4.14$ GPa, $G_{23} = 3.45$ GPa, $v_{12} = 0.3$, $\rho = 1389.23$ kg/m$^3$. Furthermore, results presented in this section are obtained neglecting the Poisson effect, i.e., assuming the structure in cylindrical bending [19], and using a shear correction factor $K = 5/6$, as well as in Refs. [15,20–22].

The first comparison is related to a simply supported beam with all layers oriented at 0°, length $L = 381$ mm, $L/h = 15$. Table 1 shows corresponding first three natural frequencies (in kHz) for the out-of-plane motion of the beam and the comparison of these results with values from literature [15,20] is extremely good.

The second comparison is related to beams with different boundary conditions, simply supported and clamped-free, symmetrically laminated (0°/90°/90°/0°) with $L/h = 15$. Table 2 lists non-dimensional natural frequencies of the beams obtained by using the proposed spectral element. A good agreement can be observed with corresponding reference values given in Ref. [15].

The third example is related to non-symmetric beams with two layers (0°/90°). Results for the first four non-dimensional natural frequencies are shown in Table 3. In this case, all the axial displacements have been constrained, so that the effect of axial-bending coupling is stronger [15]. The comparison with corresponding results from Refs. [15,21] shows a good agreement.

The last example is related to multi-span beams with different numbers of spans, both symmetric and non-symmetric lay-ups and different outer boundary conditions (even if in both cases the outer axial displacements are constrained). The corresponding first natural frequencies, expressed in kHz, are listed in Table 4 and compared to results published in Ref. [22]. For this example the comparison is extremely good.

Table 1
Out-of-plane bending natural frequencies (in kHz) for a simply supported beam (0°, $L/h = 15$, $L = 381$ mm)

| Mode | Present | [15] | [20] |
|---|---|---|---|
| 1 | 0.7551 | 0.755106 | 0.755 |
| 2 | 2.5479 | 2.547846 | 2.548 |
| 3 | 4.7160 | 4.715963 | 4.716 |

Table 2
Out-of-plane bending non-dimensional natural frequencies ($\omega L^2\sqrt{\rho/E_1h^2}$) for symmetrically laminated ($0^\circ/90^\circ/90^\circ/0^\circ$) beams ($L/h = 15$, CF = clamped-free, SS = simply-supported)

| | Mode 1 | | Mode 2 | | Mode 3 | |
|---|---|---|---|---|---|---|
| | Present | [15] | Present | [15] | Present | [15] |
| CF | 0.9240 | 0.9241 | 4.8891 | 4.8925 | 11.4351 | 11.4401 |
| SS | 2.5002 | 2.5023 | 8.4764 | 8.4813 | 15.7513 | 15.7559 |

Table 3
Non-dimensional natural frequencies ($\omega L^2\sqrt{I_0/D_{11}}$) of ($0^\circ/90^\circ$) beams with different boundary conditions ($L/h = 10$)

| | Mode | Present | [15] | [22] |
|---|---|---|---|---|
| *SS* | 1 | 8.146 | 8.13392 | 8.1439 |
| | 2 | 21.669 | 21.60865 | 21.661 |
| | 3 | 43.823 | 43.64532 | 43.788 |
| | 4 | 63.842 | 63.56258 | 63.787 |
| *CF* | 1 | 2.243 | 2.23948 | 2.2427 |
| | 2 | 12.499 | 12.46528 | 12.494 |
| | 3 | 30.478 | 30.36466 | 30.458 |
| | 4 | 50.803 | 50.61310 | 50.765 |

Table 4
First natural frequency (in kHz) for multi-span beams (with overall length $L = 30$ in) with different number of spans for symmetric and non-symmetric lay-up and different outer boundary conditions

| Spans | Simply-supported | | Clamped–clamped | |
|---|---|---|---|---|
| | Present | [22] | Present | [22] |
| $0^\circ/90^\circ/90^\circ/0^\circ$ | | | | |
| 1 | 0.1873 | 0.187 | 0.3972 | 0.397 |
| 2 | 0.7114 | 0.711 | 1.0023 | 1.002 |
| 3 | 1.4836 | 1.484 | 1.7108 | 1.711 |
| 4 | 2.4113 | 2.411 | 2.5640 | 2.564 |
| 5 | 3.4245 | 3.424 | 3.5210 | 3.521 |
| $90^\circ/0^\circ$ | | | | |
| 1 | 0.1311 | 0.131 | 0.2141 | 0.214 |
| 2 | 0.3782 | 0.378 | 0.5735 | 0.574 |
| 3 | 0.8688 | 0.869 | 1.0267 | 1.027 |
| 4 | 1.4198 | 1.420 | 1.6060 | 1.606 |
| 5 | 2.1756 | 2.176 | 2.2988 | 2.299 |

### 3.2. Numerical validation: high frequency transients

In order to validate the proposed spectral element, it has been used to evaluate the velocity at the free end of a cantilever beam under the action of an external load. This example has been already analyzed in Refs. [1,23], where results obtained by taking advantage of the FEM and of a spectral element for composite Euler–Bernoulli beams are discussed.

The cantilever beam has the following properties: length $L = 1$ m, width $b = 0.01$ m, height $h = 0.01$ m, it is made of AS/3501-6 graphite-epoxy having properties $E_1 = 144.48$ GPa, $E_2 = 9.632$ GPa, $G_{12} = G_{31} = 4.128$ GPa, $G_{23} = 3.45$ GPa, $\nu_{12} = 0.3$, $\rho = 1389$ kg/m$^3$. Moreover, the ply-stacking sequence used is $(0_5^\circ/90_5^\circ)$ to amplify the coupling between axial and bending motion. The tip load has time history and frequency spectrum shown in Fig. 2. By analyzing the corresponding figures of Refs. [1,23], and in order to obtain the same load used in these two articles, a $\sin^2$ shape has been chosen for the tip load time history, with a peak force of 4.4 N and a duration of 35 μs. This last value is different from that declared in Refs. [1,23], even though it has been chosen in order to have a frequency bandwidth of the forcing load of 44 kHz, as specified in Ref. [23]. Moreover, it must be recalled that the load shown in Fig. 2 is used to simulate an impact, so that it must give initial negative velocity at the application point. Finally, it must be stressed that, due to the very wide frequency content of this load, SEM is more efficient in the evaluation of the dynamic response than FEM that, in this case, requires 1000 finite elements to provide accurate results [1,23].

Fig. 3 shows the mid-plane velocity of the beam at the free end (i.e., $\dot{u}_0(L)$). The first peak is due to the application of the load, while the second peak is due to the wave reflected by the clamped end. The comparison of this figure with Fig. 4(a) of Ref. [1] and Fig. 2 of Ref. [23] shows a very good agreement between these results.

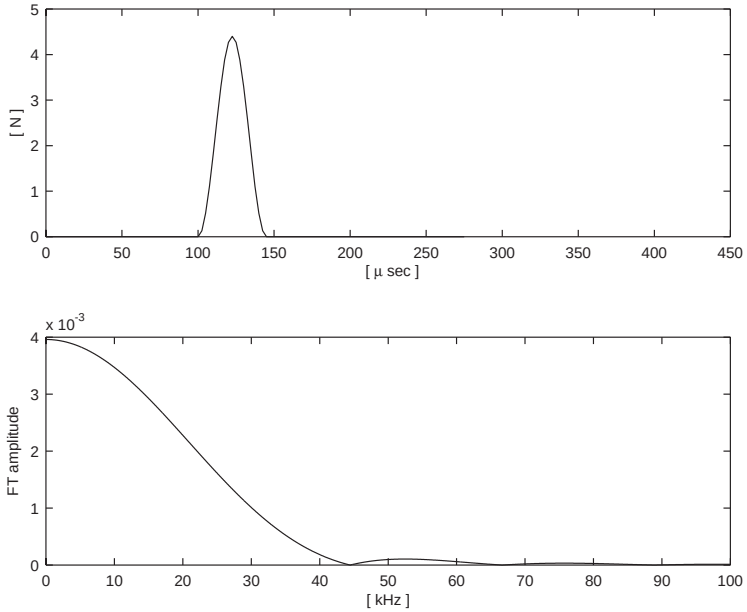


Fig. 2. Time history and amplitude of the Fourier transform of the tip load acting on a cantilever beam.

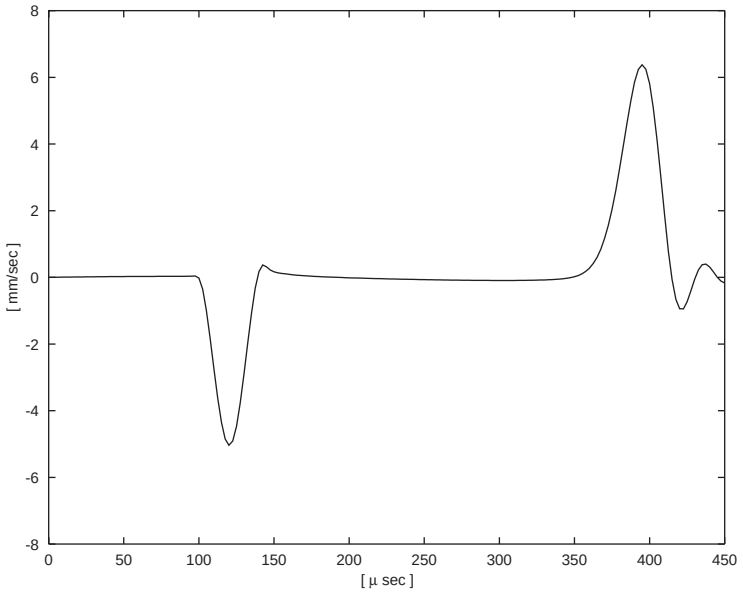


Fig. 3. Cantilever beam axial velocity due to axial tip load.

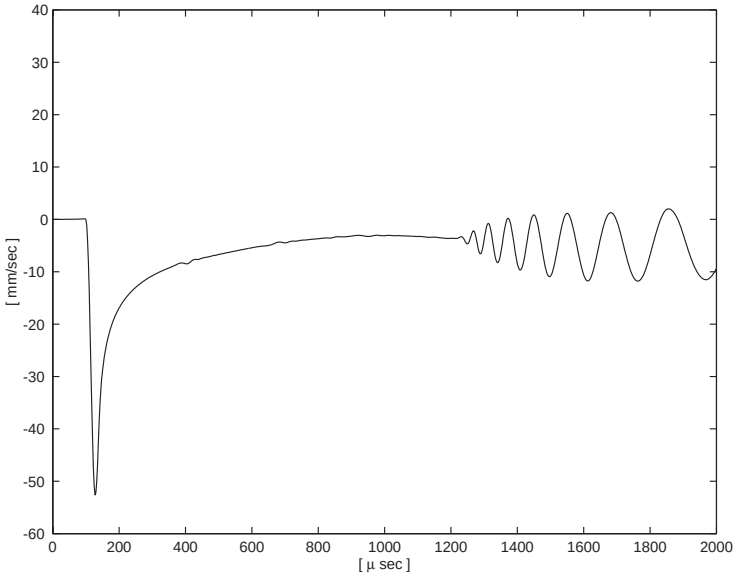


Fig. 4. Cantilever beam transverse velocity due to transverse tip load.

In Fig. 4 the out-of-plane velocity of the beam free end is shown (i.e., $\dot{w}(L)$) when the load is applied in the vertical direction. This result shows the dispersive nature of flexural waves and it is in good agreement with those shown in Refs. [1,23]. In particular, it is interesting to observe that the first reflection of waves appears at about 1200 μs, as already underlined by Chakraborty et al.

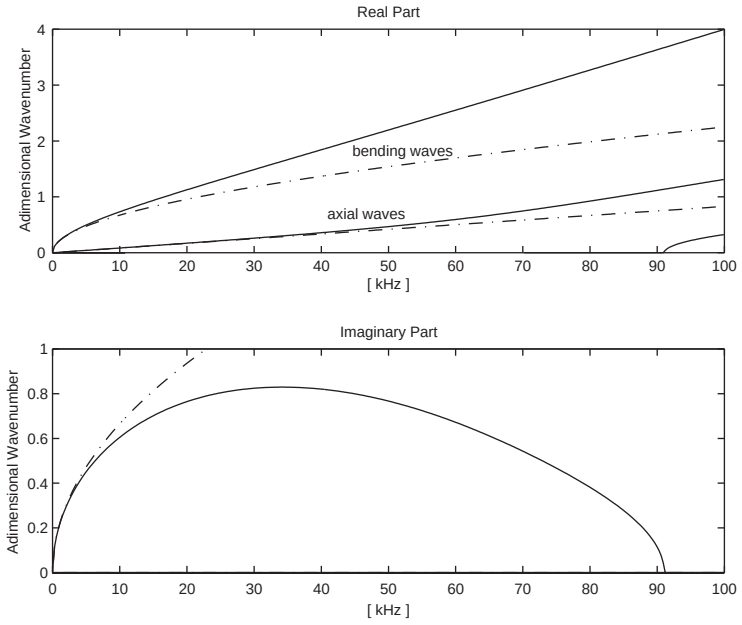


Fig. 5. Dispersion relation for the cantilever beam (—, FSDT; — · —, CLT).

[23] in the comment of their RFSDT finite element model, while the reflection predicted by the CLT model appears at about 700 μs (see Fig. 4(b) of Ref. [1] and Fig. 3 of Ref. [23]).

Discrepancies between results obtained by using CLT and FSDT are clarified by looking at the dispersion relation, shown in Fig. 5, for the beam under analysis. This figure illustrates the relation between the adimensional wavenumber (defined as $kh$) and frequency; continuous and dash-dot lines are related to FSDT and CLT respectively. Moreover, the two upper and middle curves are related to bending and axial waves respectively. Finally, it is possible to see that after 90 kHz a propagating shear mode appears.

It has been stated that the excitation bandwidth is of 44 kHz. By looking at Fig. 5 it is shown that up to 44 kHz the CLT model describes the propagation of axial waves with a sufficient accuracy, while there are large errors in the wavenumber prediction for bending waves. It follows that a FSDT approach is not necessary to determine accurately the dynamic response of the beam at the exciting horizontal force, while it is needed to evaluate the response to transverse excitation, as demonstrated by Figs. 3 and 4.

## 4. Application to pyroshock analysis

The aim of this section is to demonstrate that SEM can be very useful to predict vibrations induced by pyrotechnic charges commonly used in the space engineering. As a result, even though the comparison between dynamic properties of structures can be performed directly by comparing corresponding spectral matrices, in this article it is preferred to compare shock response spectra because this is the information required by technicians involved in pyroshock analysis.

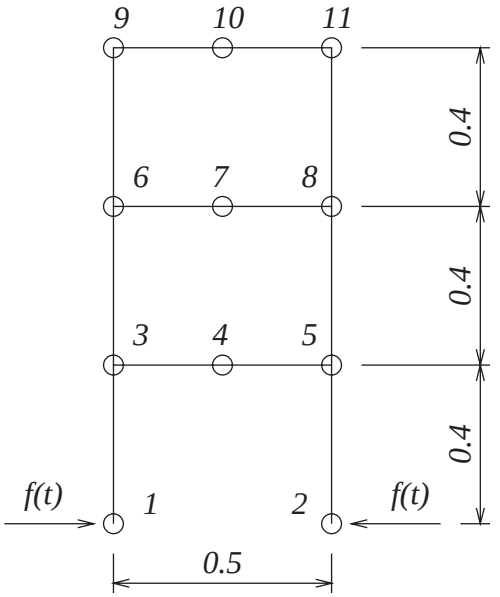


Fig. 6. The idealized satellite structure under analysis.

As already introduced in Section 1, pyroshocks are high frequency transients due to pyrotechnic devices used in aerospace engineering in order to deploy solar arrays and antennae, separate subsystems from the spacecraft or separate the spacecraft itself from the base stage booster.

The intensity of pyroshocks may be critical for some equipment. Indeed pyroshock induced vibrations have been identified as one of the major causes of in-flight satellite failures [24]. Currently, aerospace companies predict the vibration level due to pyrotechnic charges by using simple semi-empirical methods, as the one described in Ref. [25], because even though some theoretical investigations have been performed [2], a prediction methodology has not yet been established. Finally, it must be underlined that, probably, during the next years this topic will gain more attention in the scientific community, because recent launch vehicles, e.g., Ariane 5, give rise to very intense pyroshocks.

By taking advantage of the efficiency of SEM to deal with high frequency transients, in this section a two-dimensional idealized satellite structure, made of sandwich beams, is analyzed to determine its shock response spectrum (SRS)[1] to an excitation typical of a pyrotechnic charge called 'separation nut'.

The structure under analysis is shown in Fig. 6 (where dimensions are expressed in m) and it is assumed that equipment, to be connected to nodes 4, 7 and 10, will be sensitive to out-of-plane vibrations of the supporting beam. The whole structure is made of sandwich panels with composite faces and aluminium honeycomb core with properties: $E_1 = 120$ GPa, $E_2 = E_3 = 7.9$ GPa, $G_{12} = G_{23} = G_{31} = 5.5$ GPa, $\nu = 0.3$, $\rho = 1580$ kg/m$^3$ and $G_{13} = 140.7$ MPa, $G_{23} =$

[1] According to Ref. [3], SRS is defined as the maximum absolute acceleration response of a series of damped, single-d.o.f. oscillators to the application of the acceleration time history to their base, plotted over a specified frequency range of oscillator natural frequencies and a constant quality factor $Q$ ($Q = 1/2\zeta$), where $\zeta$ is viscous damping ratio.

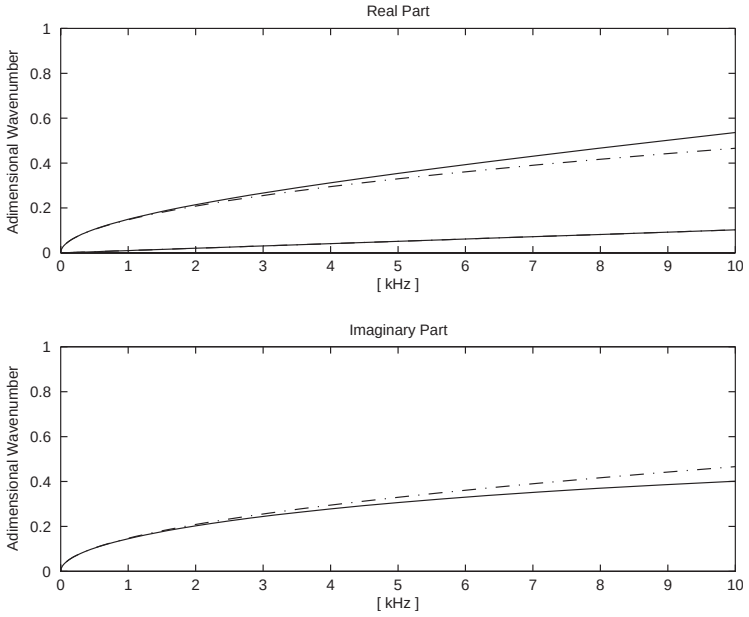


Fig. 7. Dispersion relation for the sandwich beam with thin core (—, FSDT; — · —, CLT).

70.35 MPa, $\rho = 34.15\ \mathrm{kg/m^3}$ for composite faces and core respectively. Both faces have a thickness of 1 mm and are made by two equal layers, moreover the orientation of the various laminae is $(0^\circ/90^\circ/\mathrm{core}/90^\circ/0^\circ)$. Finally, two core thicknesses are considered: 8 and 18 mm and, according to Ref. [26], an overall structural damping $\eta = 1.2\%$ has been selected, constant with respect to frequency. As a result, damping of the honeycomb structure has been considered by multiplying the dynamic stiffness matrix, $[K_d]$, by $(1 + \mathrm{j}\eta)$.

Dispersion relations for the structures with thin and thick core are shown in Figs. 7 and 8 respectively. Both figures permit a comparison between the predictions using FSDT and CLT, denoted by continuous and dash-dot line respectively, for bending and axial waves. It appears that CLT predicts with sufficient accuracy the propagation of bending waves up to about 2 and 1 kHz for the structures with thin and thick core respectively. Since the propagation of bending waves is of paramount importance for the analysis described in this section, and the excitation bandwidth covers several kHz, it follows that in the following only results obtained by using FSDT, i.e., the spectral element proposed in this article, are described.

It is assumed that separation nuts are acting at nodes 1 and 2 of the structure under analysis, so that their effect is represented by two forces with a time history as shown in Fig. 9 and given by the following relation:

$$f(t) = \begin{cases} -0.4\sin^2\left(\frac{2\pi}{T_1}(t - \Delta t_1)\right), & t \in [\Delta t_1, \Delta t_1 + T_1], \\ \sin\left(\frac{2\pi}{T_2}(t - \Delta t_1 - T_1)\right), & t \in [\Delta t_1 + T_1, \Delta t_1 + T_1 + T_2], \end{cases} \tag{22}$$

where $T_1 = T_2 = 500\ \mu\mathrm{s}$ have been determined from Fig. 7 of Ref. [26] showing the measured time histories of the separation nuts, and $\Delta t_1 = 1500\ \mu\mathrm{s}$. Finally, in order to obtain results of general validity, the excitation force $f(t)$ has been normalized so that its maximum is equal to 1 N.

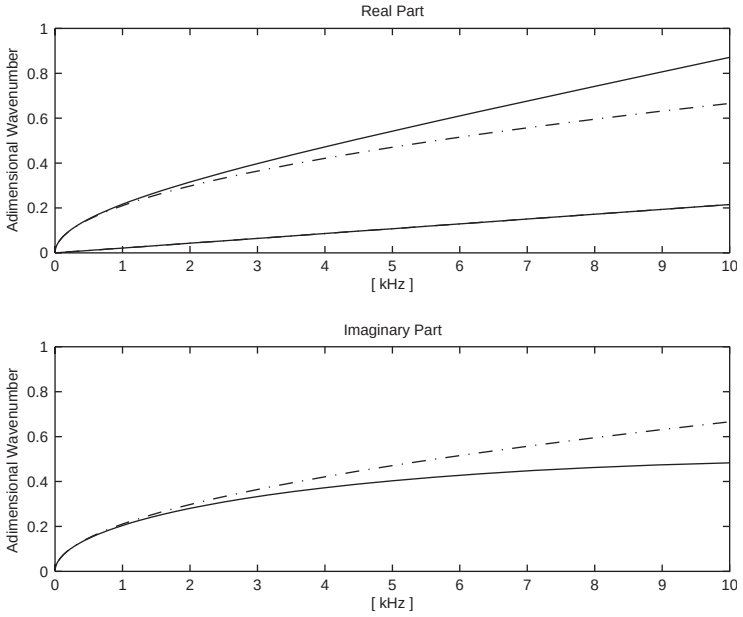


Fig. 8. Dispersion relation for the sandwich beam with thick core (—, FSDT; — · —, CLT).

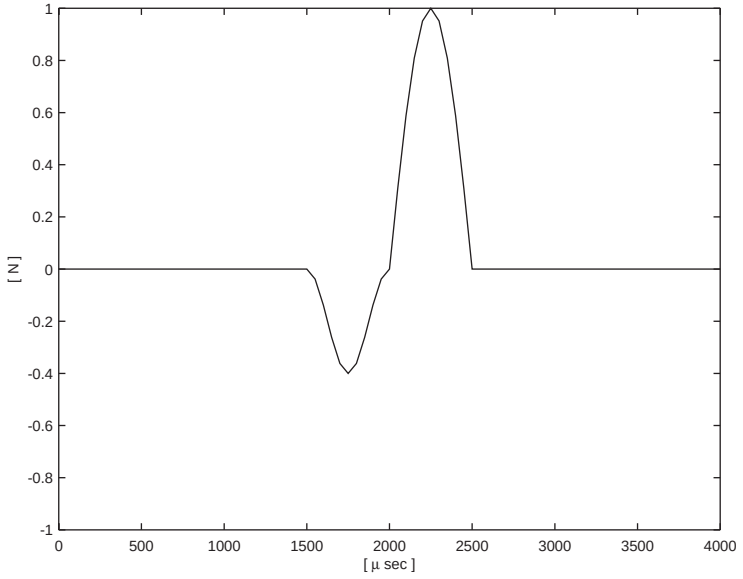


Fig. 9. Time history of the exciting force.

Both structures, i.e., with thin and thick cores, are built by connecting several sandwich beams. It follows that the analysis has been performed by evaluating the Fourier transform of dynamic responses as the product between the fast Fourier transform of $f(t)$ and the spectral matrix of the

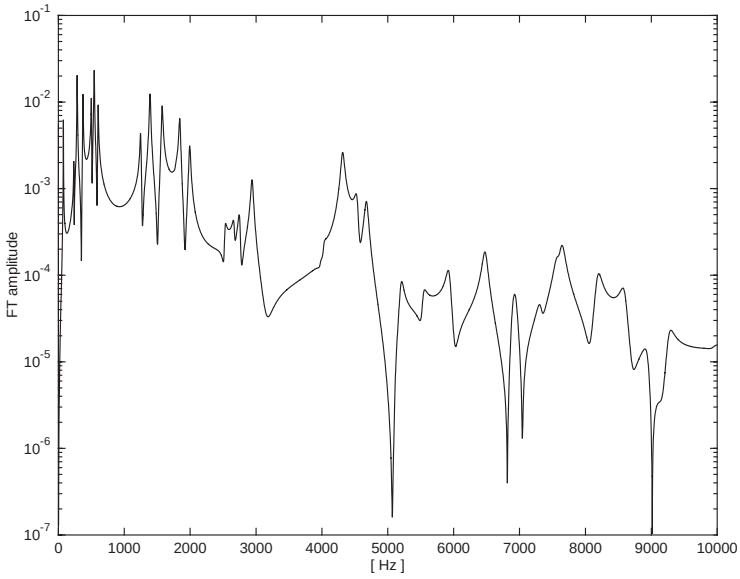


Fig. 10. FT of the out-of-plane acceleration at node 4 (thin core).

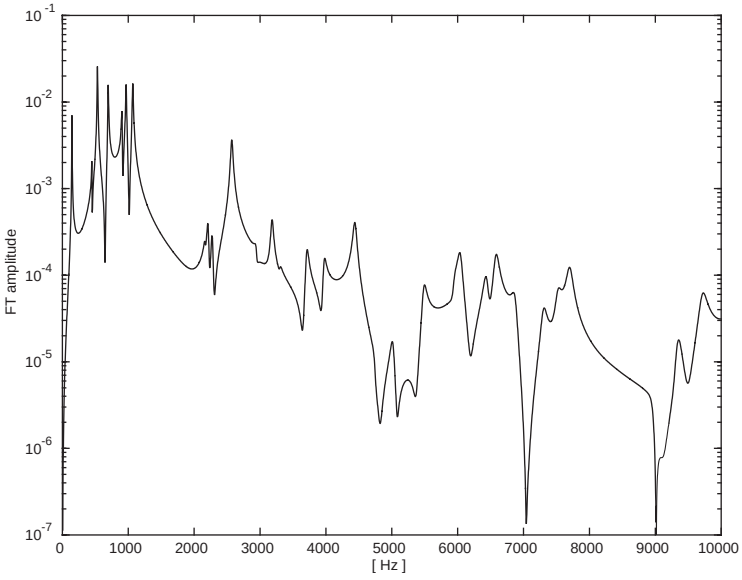


Fig. 11. FT of the out-of-plane acceleration at node 4 (thick core).

whole structure (the simulation was run by using 10 000 sample points in time and a frequency resolution of 2 Hz).

Figs. 10 and 11 show the fast Fourier transform of the out-of-plane acceleration at node 4 for thin and thick core respectively. Since the spectrum of the exciting force is almost flat at low

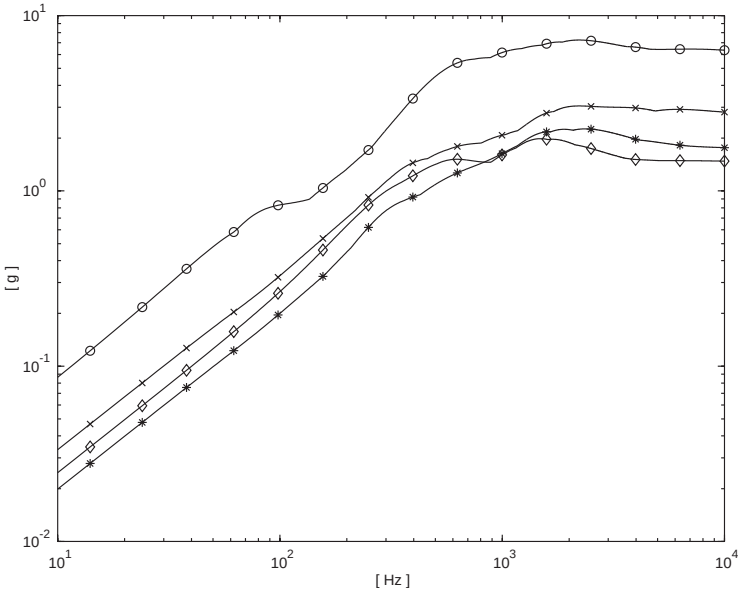


Fig. 12. SRS at nodes 2 (—○—), 4 (—×—), 7 (—∗—) and 10 (—◇—) (thin core).

frequencies, from these figures it is verified that the structure with thick core has natural frequencies higher than that with thin core.

Subsequently, SRS are evaluated by applying the time history (calculated by using the inverse fast Fourier transform) of dynamic responses at the base of a series of single-d.o.f. oscillators with different natural frequency and constant quality factor $Q = 10$, i.e., $\zeta = 5\%$, according to Ref. [3].

Figs. 12 and 13 show, for thin and thick core, respectively, the SRS at nodes 2, 4, 7 and 10, i.e., at the excitation point and at locations where equipment should be placed. Both figures highlight a great reduction in the SRS moving away from the excitation point, while differences between the environments at nodes 4, 7 and 10 are of lower extent. Furthermore, it is shown that for both structures acceleration levels at nodes 7 and 10 are similar, even if lower than corresponding levels at node 4.

Table 5 summarizes SRS prevailing results, i.e., acceleration levels at both low (100 Hz) and high frequency (maximum SRS after the constant velocity line) as well as the residual SRS percentage, i.e., the ratio between the SRS at the considered location and at the source (node no. 2). It shows that, as can be expected, the structure with the thicker core gives lower acceleration levels and the interesting results that the residual SRS differ by no more than 5–6% between the two structures, even though there is a big difference between the thickness of the two cores.

## 5. Conclusions

In this article a spectral element matrix for anisotropic, laminated composite beams is presented. It is based on the First order Shear Deformation Theory, so that it takes into account

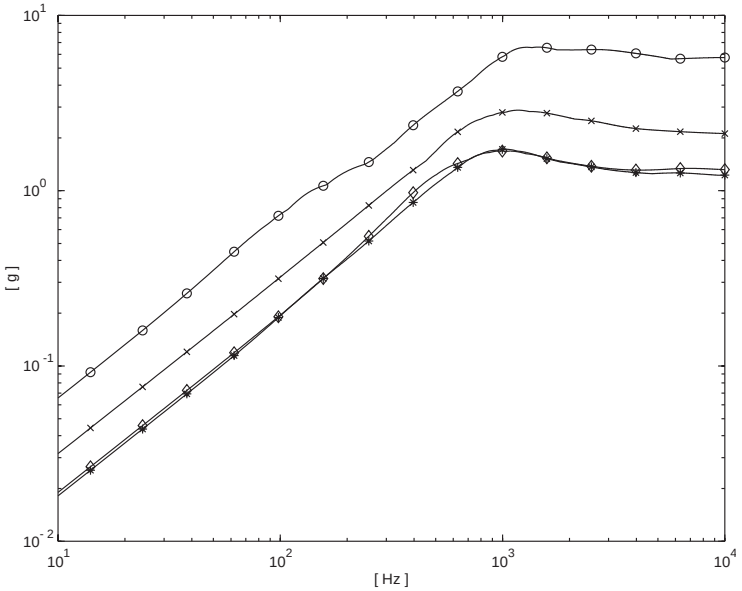


Fig. 13. SRS at nodes 2 (—○—), 4 (—×—), 7 (—∗—) and 10 (—◇—) (thick core).

Table 5
SRS levels at several nodes of the frame structure under analysis

| | Thin core | | | | Thick core | | | |
|---|---|---|---|---|---|---|---|---|
| | Low freq. | | High freq. | | Low freq. | | High freq. | |
| Node no. | Accel. ($g$) | Residue (%) | Accel. ($g$) | Residue (%) | Accel. ($g$) | Residue (%) | Accel. ($g$) | Residue (%) |
| 2 | 0.81 | 100 | 7.09 | 100 | 0.72 | 100 | 6.40 | 100 |
| 4 | 0.32 | 40 | 2.98 | 42 | 0.32 | 44 | 2.80 | 44 |
| 7 | 0.20 | 25 | 2.20 | 31 | 0.19 | 26 | 1.66 | 26 |
| 10 | 0.26 | 32 | 1.95 | 27 | 0.19 | 26 | 1.66 | 26 |

both the shear deformation as well as rotatory inertia, whose effects can be very important at high frequencies. The spectral matrix is derived by considering the propagation of waves into the structural media and solving the corresponding wave equation.

In order to validate the proposed spectral element, a number of comparisons with data from the scientific literature are shown: it is demonstrated that it predicts accurately natural frequencies of beams with different boundary conditions, as well as eigenfrequencies of beams on multiple spans. Comparisons with results obtained by using the dynamic stiffness matrix (SDM) confirm that SEM and SDM are equivalent, at least for beams, and that differences in the predictions are due to numerical errors. Furthermore, a comparison demonstrates the accuracy of SEM in the prediction of the dynamic response to high frequency transients.

Finally, the proposed spectral element has been employed to demonstrate that it can be very useful to perform pyroshock analysis. An idealized satellite structure made by sandwich beams has been analyzed, and the shock response spectrum evaluated at several locations.

Future investigations can take advantage of the proposed spectral element in order to analyze the effect of several parameters, e.g., geometrical discontinuities such as different overall thicknesses of the beams, optimize connections, analyze and optimize the location of damping layers.

## Acknowledgements

The author would like to thank Dr. P.C. Marucchi Chierro from Alenia Spazio for very useful discussions about pyroshock analysis.

## References

[1] D.R. Mahapatra, S. Golapakrishnan, T.S. Sankar, Spectral-element-based solutions for wave propagation analysis of multiply connected unsymmetric laminated composite beams, *Journal of Sound and Vibration* 237 (5) (2000) 819–836.
[2] H. Himelblau, J.E. Manning, D.L. Kern, A.G. Piersol, S. Rubin, *Dynamic Environmental Criteria*, NASA Technical Handbook 7005, 2001.
[3] NASA Technical Standard, *Pyroshock Test Criteria*, NASA-STD-7003, 1999.
[4] L. Cremer, M. Heckl, E.E. Ungar, *Structure-Borne Sound—Structural Vibrations and Sound Radiation at Audio Frequencies*, 2nd Edition, Springer, Berlin, 1988.
[5] J.F. Doyle, *Wave Propagation in Structures—Spectral Analysis Using Fast Discrete Fourier Transforms*, 2nd Edition, Springer, Berlin, 1997.
[6] S.R. Marur, T. Kant, On the performance of higher order theories for transient dynamic analysis of sandwich and composite beams, *Computers & Structures* 65 (5) (1997) 741–759.
[7] S.R. Marur, T. Kant, Transient dynamics of laminated beams: an evaluation with a higher-order refined theory, *Composite Structures* 41 (1998) 1–11.
[8] J.N. Reddy, *Mechanics of Laminated Composite Plates: Theory and Analysis*, CRC Press, Boca Raton, FL, 1997.
[9] J.R. Vinson, R.L. Sierakowski, *The Behavior of Structures Composed of Composite Materials*, Martinus Nijhoff, Dordrecht, 1987.
[10] K. Kraus, *Thin Elastic Shells*, Wiley, New York, 1967.
[11] R.M. Jones, *Mechanics of Composite Materials*, McGraw-Hill, New York, 1975.
[12] J.N. Reddy, Theory and analysis of laminated composite plates and shells, *Proceedings of Mechanics of Composite Materials and Structures Conference*, Portugal, 1998, pp. 1–87.
[13] M. Di Sciuva, Improved shear-deformation theory for moderately thick shells and plates, *Journal of Applied Mechanics* 54 (1987) 589–596.
[14] A.Y.T. Leung, *Dynamic Stiffness and Substructures*, Springer, Berlin, 1993.
[15] M. Eisenberger, H. Abramovich, O. Shulepov, Dynamic stiffness analysis of laminated beams using a first order shear deformation theory, *Composite Structures* 31 (1995) 265–271.
[16] H. Abramovich, M. Eisenberger, O. Shulepov, Vibrations and buckling of cross-ply nonsymmetric laminated composite beams, *American Institute of Aeronautics and Astronautics Journal* 34 (5) (1996) 1064–1069.
[17] A.Y.T. Leung, W.E. Zhou, Dynamic stiffness analysis of laminated composite plates, *Thin-Walled Structures* 25 (2) (1996) 109–133.
[18] U. Lee, J. Kim, Dynamics of elastic-piezoelectric two-layer beams using spectral element method, *International Journal of Solids and Structures* 37 (2000) 4403–4417.
[19] J.M. Whitney, Cylindrical bending versus beam theory in the analysis of composite laminates, *Composites* 26 (1995) 395–398.
[20] K. Chandrashekhara, K. Krishnamurthy, S. Roy, Free vibration of composite beams including rotary inertia and shear deformation, *Composite Structures* 14 (1990) 269–279.

[21] H. Abramovich, A. Livshits, Free vibrations of non-symmetric cross ply laminated composite beams, *Journal of Sound and Vibration* 176 (5) (1994) 597–612.
[22] H. Abramovich, M. Eisenberger, O. Shulepov, Vibrations of multi-span non-symmetric composite beams, *Composites Engineering* 5 (1995) 397–404.
[23] A. Chakraborty, D.R. Mahapatra, S. Gopalakrishnan, Finite element analysis of free vibration and wave propagation in asymmetric composite beams with structural discontinuities, *Composite Structures* 55 (2002) 22–36.
[24] C. Moening, S. Rubin, Pyrotechnic shocks, *Proceedings of the 56th Shock & Vibration Symposium*, Monterey, CA, 1985.
[25] W.J. Kacena III, M.B. McGrath, W.P. Rader, *Aerospace Systems Pyrotechnic Shock Data*, *Vol. VI—Pyrotechnic Shock Design Guidelines Manual*, Martin Marietta Corporation, 1970.
[26] Y.A. Lee, W. Henricks, Pyroshock analysis and test of composite satellite structure, American Institute of Aeronautics and Astronautics Paper 92-02-167, 1992.